

THE EFFECT OF ACTIVE GALACTIC NUCLEI ON THE MID-INFRARED AROMATIC FEATURES

ALEKSANDAR M. DIAMOND-STANIC¹, GEORGE H. RIEKE¹

Accepted for publication in ApJ on 13 September 2010

ABSTRACT

We present Spitzer measurements of the aromatic (also known as PAH) features for 35 Seyfert galaxies from the revised Shapley–Ames sample and find that the relative strengths of the features differ significantly from those observed in star-forming galaxies. Specifically, the features at 6.2, 7.7, and 8.6 μm are suppressed relative to the 11.3 μm feature in Seyferts. Furthermore, we find an anti-correlation between the $L(7.7\ \mu\text{m})/L(11.3\ \mu\text{m})$ ratio and the strength of the rotational H_2 emission, which traces shocked gas. This suggests that shocks suppress the short-wavelength features by modifying the structure of the aromatic molecules or destroying the smallest grains. Most Seyfert nuclei fall on the relationship between aromatic emission and $[\text{Ne II}]$ emission for star-forming galaxies, indicating that aromatic-based estimates of the star-formation rate in AGN host galaxies are generally reasonable. For the outliers from this relationship, which have small $L(7.7\ \mu\text{m})/L(11.3\ \mu\text{m})$ ratios and strong H_2 emission, the 11.3 μm feature still provides a valid measure of the star-formation rate.

Subject headings: galaxies: active, galaxies: nuclei, galaxies: Seyfert, galaxies: ISM

1. INTRODUCTION

The mid-infrared (mid-IR) aromatic emission features are a universal product of star formation in moderate-to-high-metallicity galaxies (e.g., Roche et al. 1991; Lu et al. 2003; Smith et al. 2007a). Their molecular carriers, often assumed to be polycyclic aromatic hydrocarbons (PAHs, Leger & Puget 1984; Allamandola et al. 1985; Tielens 2008), radiate through IR fluorescence following vibrational excitation by a single ultraviolet (UV) photon (Tielens 2005) and provide an indirect measurement of the UV radiation field strength, and therefore the star-formation rate (SFR), that is largely extinction independent (e.g., Peeters et al. 2004; Calzetti et al. 2007; Rieke et al. 2009). This emission is thought to originate in photo-dissociation regions where aromatic molecules are shielded from the harsh radiation field near hot stars (e.g., Povich et al. 2007). These molecules can also be destroyed by the harder radiation field associated with an active galactic nucleus (AGN, Voit 1992; Genzel et al. 1998). Nonetheless, aromatic features are readily detected in many AGNs above IR continua boosted by hot dust, and they have been used to probe the SFR in AGN host galaxies (e.g., Schweitzer et al. 2006; Shi et al. 2007, 2009; Lutz et al. 2008). Understanding what environments destroy or modify these features is important for constraining systematic uncertainties in aromatic-based estimates of the SFR, and is a key way to probe the nature of their molecular carriers, an open issue in our understanding of the interstellar medium.

Duley & Williams (1981) first suggested that vibrational modes of aromatic hydrocarbons could produce the observed features, which were subsequently identified with specific C–H and C–C bending and stretching modes (Allamandola et al. 1989). Specifically, the 6.2 and 7.7 μm features are produced by C–C stretching modes, the 8.6 μm feature by C–H in-plane bending modes, and the 11.3 and 12.7 μm features by C–

H out-of-plane bending modes. While these features are commonly attributed to PAHs, we use the simpler, more general term “aromatic” to avoid making assumptions about the detailed structure of the molecules. It is worth noting, for example, that PAH spectra from laboratory measurements and quantum chemical calculations are unable to match the range of astronomical spectra without artificial enhancements of the 6.2, 7.7, and 8.6 μm feature strengths (e.g., Li & Draine 2001). Regardless of this uncertainty associated with uniquely matching observed spectra with expectations for specific molecules, one can probe the properties of the aromatic carriers by measuring the relative strengths of the emission features, which are expected to vary as a function of charge state (e.g., Bakes et al. 2001), molecular size (e.g., Draine & Li 2001), and molecular structure (e.g., Vermeij et al. 2002).

Efforts to study variations in aromatic feature strengths outside the Milky Way have focused on star-forming galaxies (e.g., Smith et al. 2007a; Galliano et al. 2008; Roseboom et al. 2009; O’Dowd et al. 2009), but the AGNs included in these studies have shown evidence for suppression of shorter wavelength features (e.g., those at 6.2, 7.7, and 8.6 μm) relative to those at longer wavelengths. For example, Smith et al. (2007a) studied a sample of 59 galaxies from the Spitzer Infrared Nearby Galaxy Survey (SINGS, Kennicutt et al. 2003), of which 12 have Seyfert nuclei and 20 have low-ionization nuclear emission-line regions (LINERs), and they found a tendency for the systems with reduced 6–8 μm features to be associated with low-luminosity AGNs. They speculated on possible causes for this behavior, including whether the AGN can modify the aromatic grain size distribution or serve as the excitation source for aromatic emission. Similarly, O’Dowd et al. (2009) studied a sample of 92 galaxies at $z \sim 0.1$ from the Spitzer SDSS GALEX Spectroscopic Survey, including eight AGN-dominated and 20 composite systems, and found that the AGNs exhibited lower 7.7/11.3 μm ratios. They interpreted this behavior as being consistent with destruction of small aromatic

¹ Steward Observatory, University of Arizona, Tucson, AZ, 85721

molecules by shocks or X-rays associated with the AGNs, but they were unable to distinguish any differences between the AGN-dominated and composite objects, nor any strong correlation with AGN power. The physical slit size at their median redshift is 6 kpc, so there is little spatial information.

In this paper we analyze the aromatic features drawing from the sample of 89 local Seyfert galaxies studied by Diamond-Stanic et al. (2009). This sample is from the revised Shapley-Ames catalog (RSA, Sandage & Tammann 1987), and includes every galaxy brighter than $B_T = 13$ that is known to host Seyfert activity (Maiolino & Rieke 1995; Ho et al. 1997). The median distance of the sample is 22 Mpc, so the $3.7''$ slit width of the Short-Low (SL) module of the Infrared Spectrograph (IRS, Houck et al. 2004) on the Spitzer Space Telescope (Werner et al. 2004) provides spatial information on scales of a few hundred parsecs, allowing us to isolate nuclear regions distinct from the rest of the galaxy. As a result, we are able to probe the effect of AGNs on the aromatic features more systematically than has previously been done.

2. DATA

We gathered data from the Spitzer archive taken with the IRS SL module ($\lambda = 5.2\text{--}14.5\ \mu\text{m}$, $R = 64\text{--}128$) from a variety of programs (24, 86, 159, 668, 3247, 3269, 3374, 30471, 30572, 30577, 30745, 40018, and 50702), as well as dedicated data taken for this study (program 40936, PI: G. H. Rieke). We use CUBISM (Smith et al. 2007b) to extract one-dimensional spectra from the basic calibrated data using $3.6'' \times 7.2''$ apertures oriented along the slit direction. This aperture size was chosen to isolate the nuclear component of the aromatic emission while still including a substantial fraction of the diffraction-limited beam. We use the calibration for extended sources based on the assumption that the regions producing aromatic emission are spatially extended, so the extracted spectra are in units of surface brightness. We use overlapping data in the $7.59\text{--}8.42\ \mu\text{m}$ region to scale the SL2/SL3 orders to the SL1 order when offsets are apparent; these offsets are $< 10\%$ in all cases.

We then use a modified version of PAHFIT (Smith et al. 2007a) to determine the strength of the various aromatic features. This spectral fitting package includes aromatic features represented by Drude profiles, dust continuum emission represented by modified blackbodies at fixed temperatures, fine-structure lines and H_2 rotational lines represented by Gaussian profiles, starlight represented by $T = 5000\ \text{K}$ blackbody emission, and dust extinction represented by a power-law and silicate features. Because Seyfert galaxies exhibit higher-ionization emission lines, silicate dust emission, and hot-dust continuum emission, we additionally include a $[\text{Ne VI}] \lambda 7.652\ \mu\text{m}$ emission line and a silicate emission component, both represented by Gaussian profiles, and we use temperatures of 1000, 750, 500, 350, 225, 150, and 100 K for the dust continuum emission. We show example PAHFIT decompositions for three sources exhibiting a range in continuum shape and silicate extinction in Figure 1.

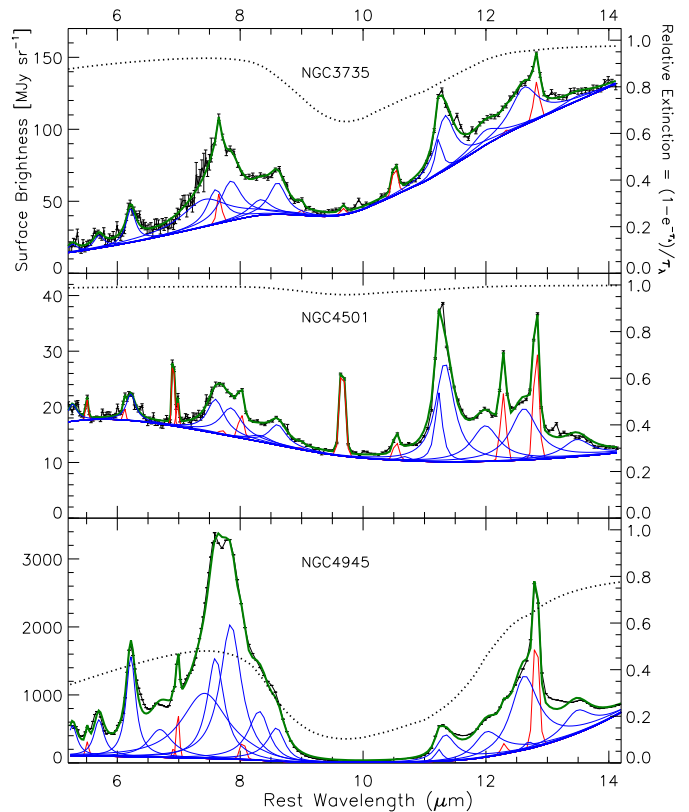


FIG. 1.— Example PAHFIT spectral decompositions for three RSA Seyfert nuclei. The observed spectra are shown in black. The blue lines above the continuum correspond to the aromatic features, while red lines correspond to unresolved atomic and molecular emission lines. The total fit is shown in green, and the dotted line indicates the extinction profile.

3. RESULTS

The data exhibit a range of signal-to-noise ratios (S/N), so we visually inspected all of the nuclear spectra to identify those that have clear detections of the relevant aromatic features and whose spectra are adequately described by the PAHFIT model. The spectra for these 35 sources are shown in Figure 2. Since many of the observations were executed with the mapping mode of IRS, it is also possible to extract spectra for off-nuclear regions in some galaxies, allowing for comparison between spectra dominated by the active nucleus and spectra dominated by H II regions within the same galaxy. We identified off-nuclear regions that were covered by the IRS slit and had sufficient S/N to detect the relevant aromatic features in 21/35 galaxies. We show a comparison between the nuclear and off-nuclear extractions for these galaxies in Figure 3, and we compile relevant measurements in Tables 1 and 2.

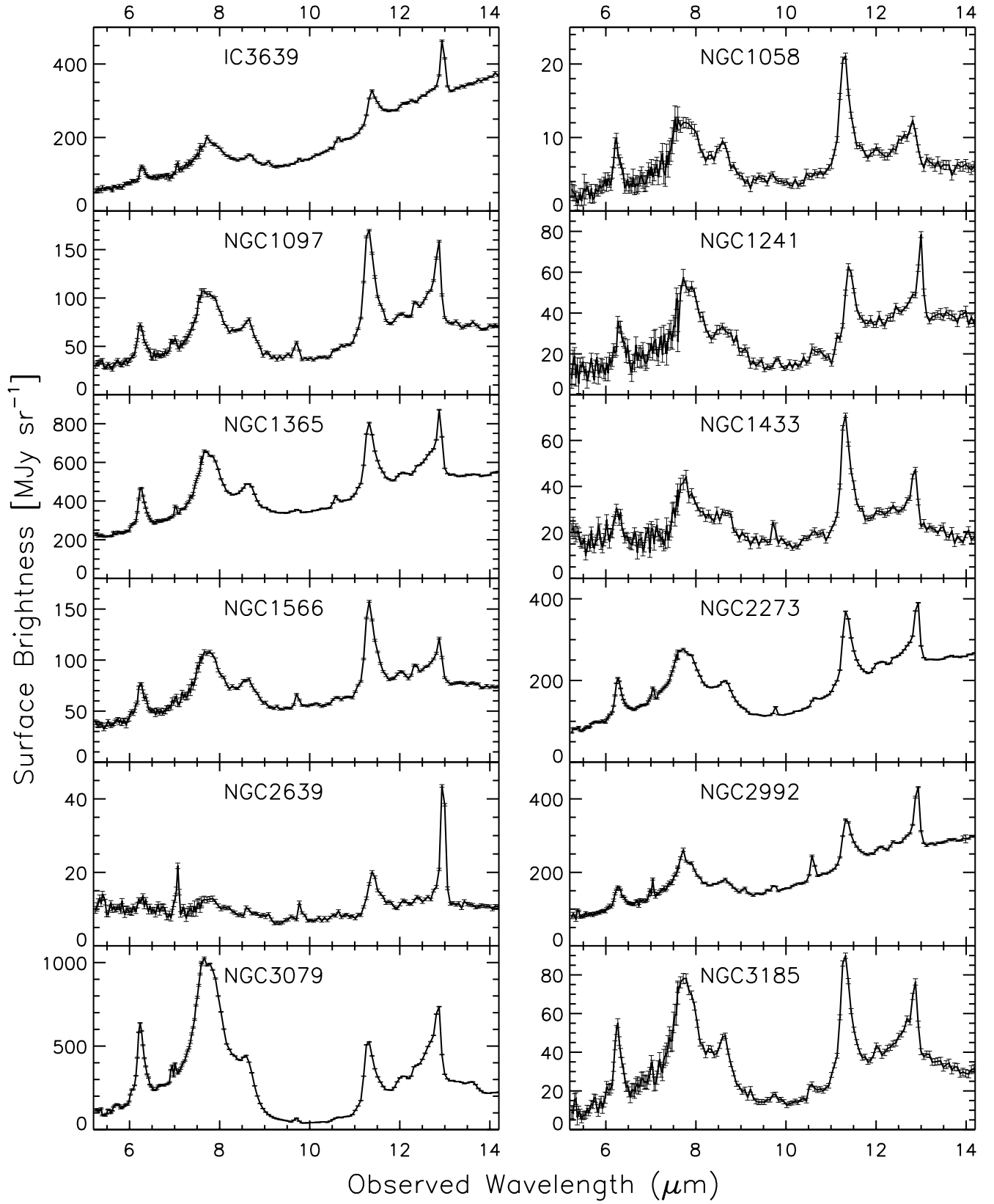
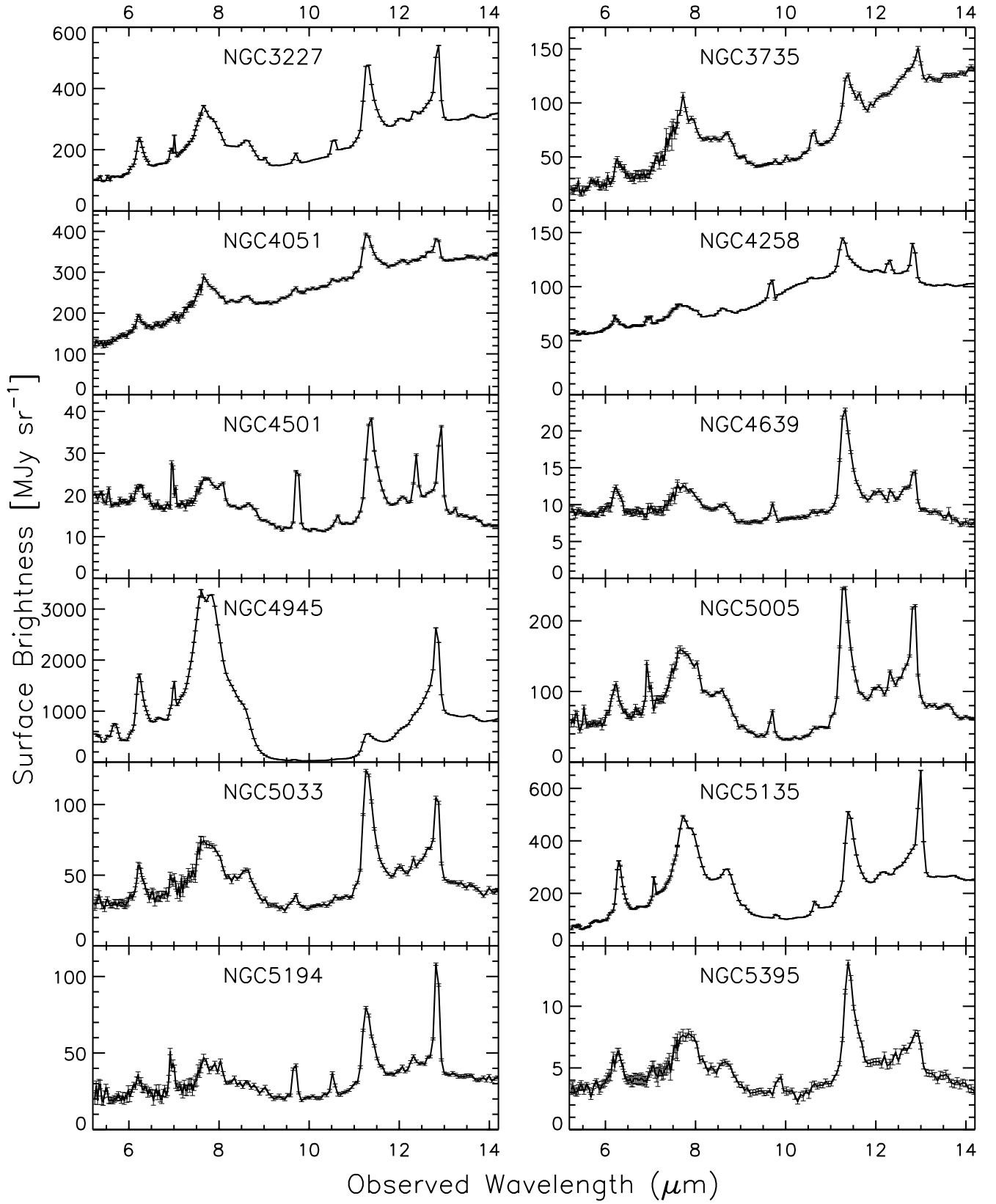
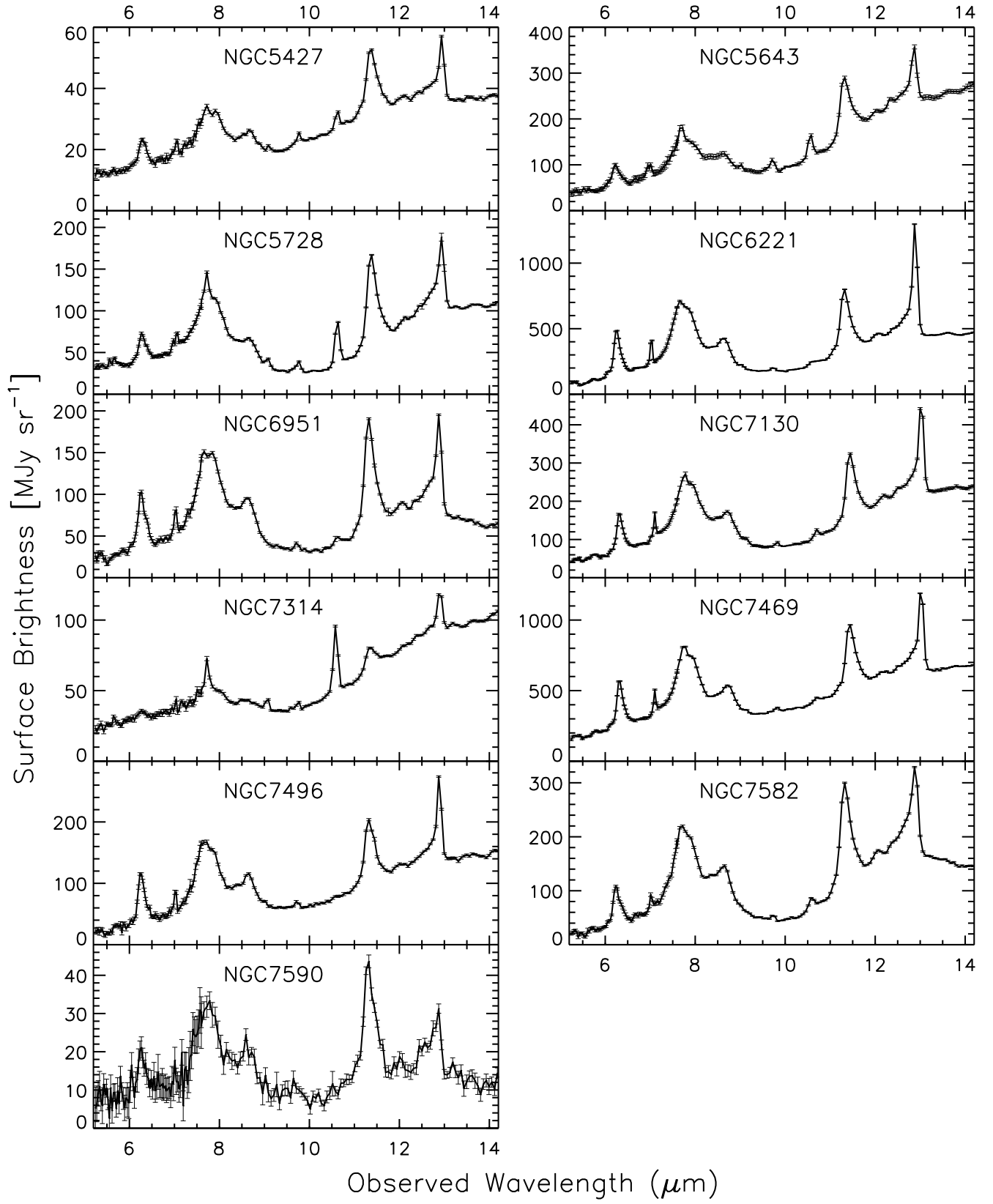


FIG. 2.— Low-resolution 5.2–14.2 μm Spitzer/IRS nuclear spectra for the 35 RSA Seyfert galaxies considered in this study.

FIG. 2.— *Continued*

FIG. 2.— *Continued*

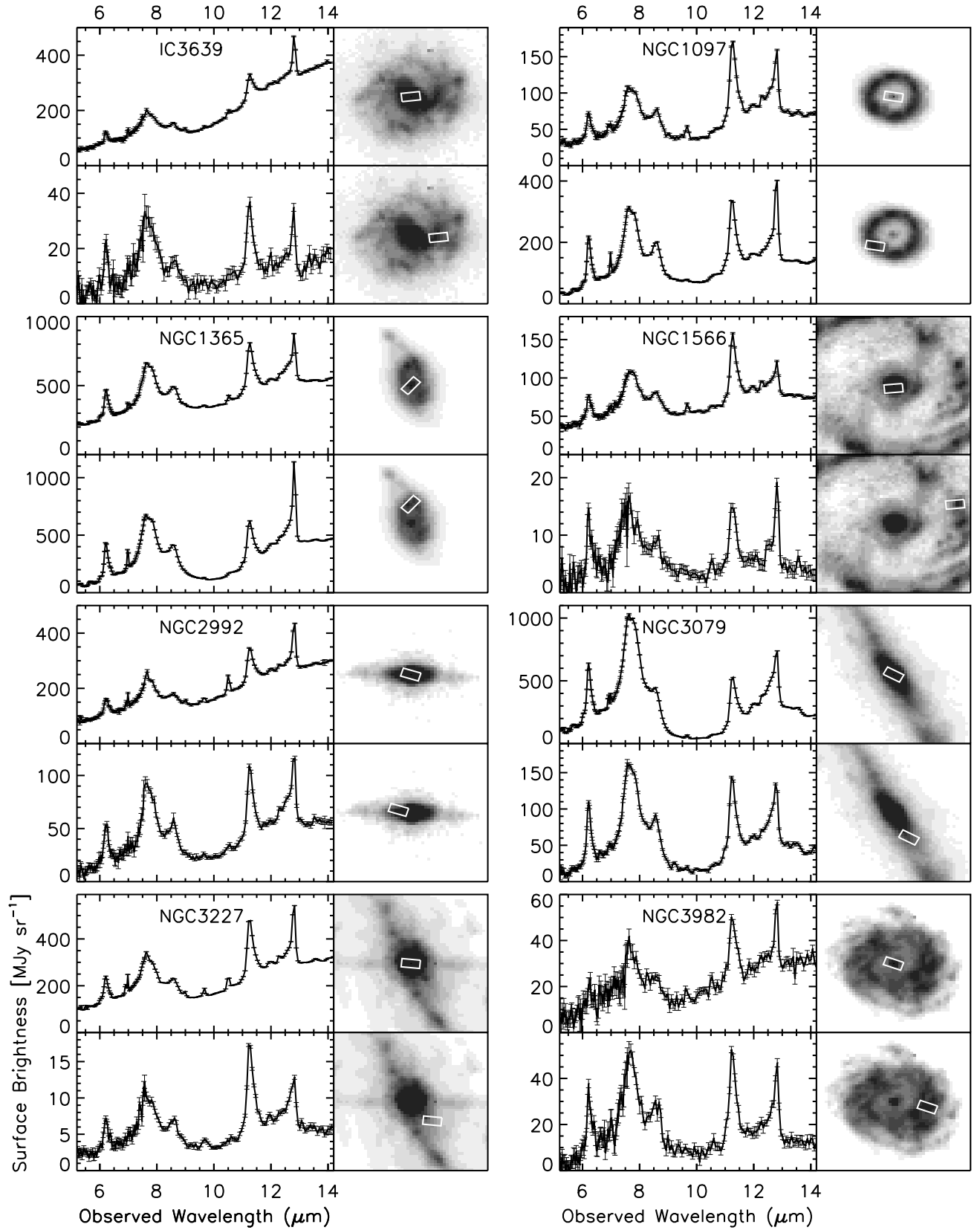
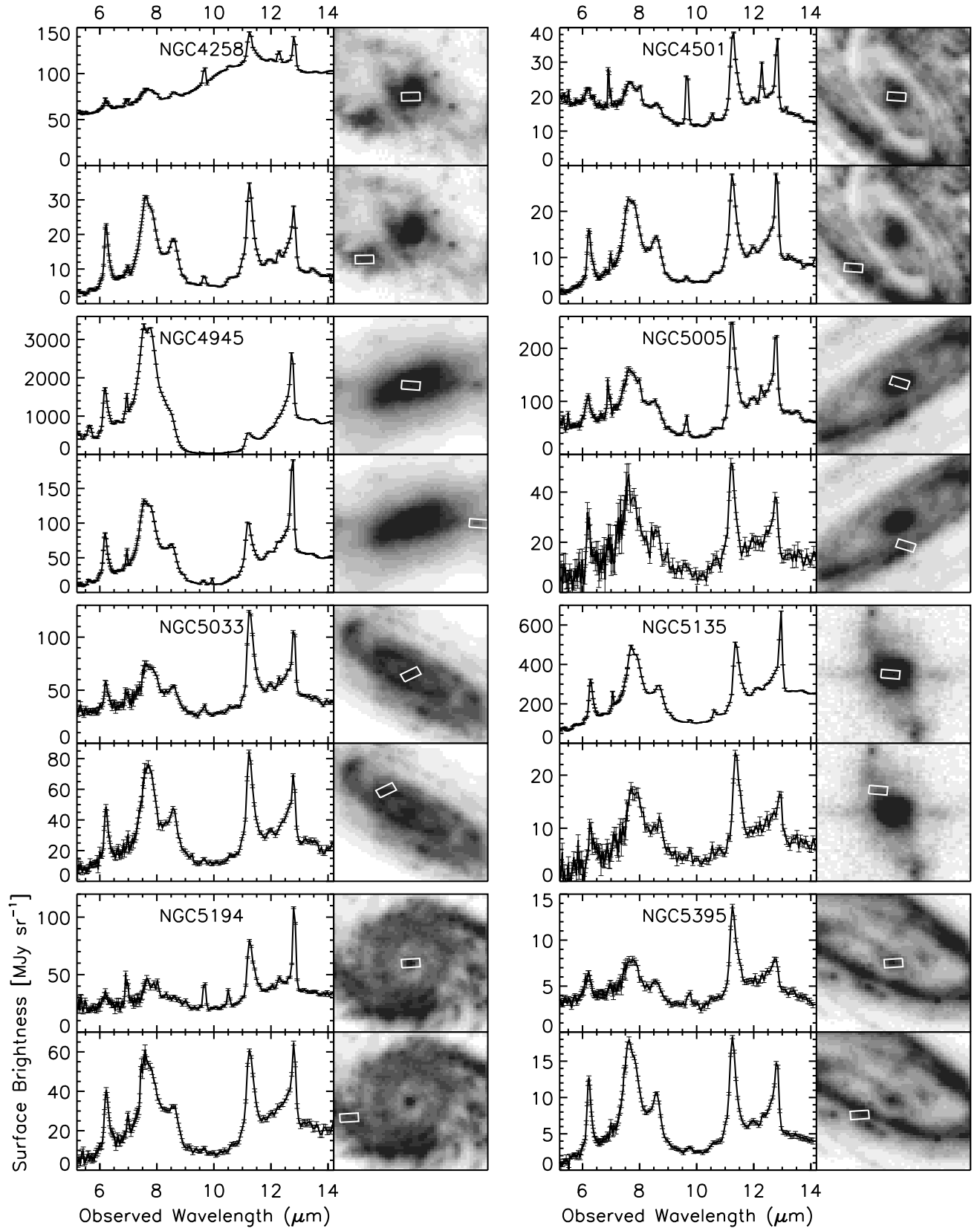
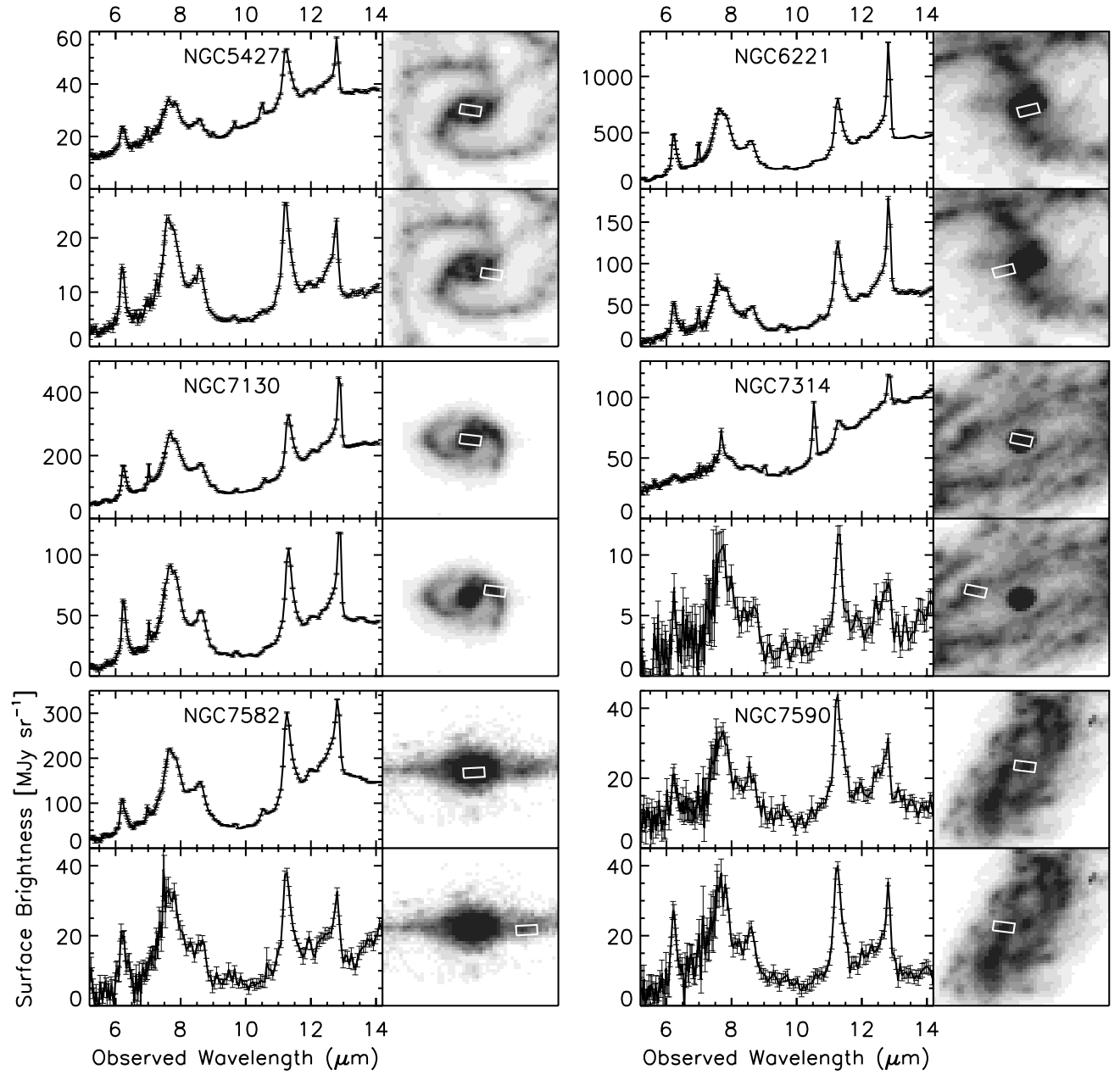


FIG. 3.— Nuclear and off-nuclear spectra for the 21/35 Seyfert galaxies where off-nuclear regions were covered by the IRS slit and had sufficient S/N to detect the relevant aromatic features. The panel to the right of each spectrum shows the corresponding $3.6'' \times 7.2''$ extraction region overlaid on the central $1' \times 1'$ of an IRAC $8.0 \mu\text{m}$ image.

FIG. 3.— *Continued*

FIG. 3.— *Continued*

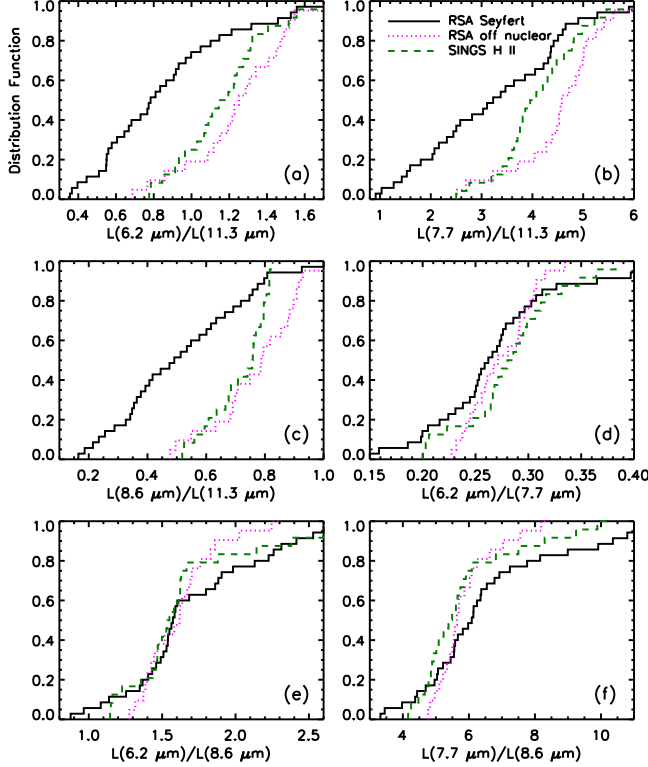


FIG. 4.— The cumulative distribution of aromatic feature ratios for 35 RSA Seyfert nuclei, 21 off-nuclear regions, and 27 SINGS H II galaxies. The first three panels show that the 6.2, 7.7, and 8.6 μm features are systematically weaker relative to the 11.3 μm feature for the Seyfert nuclei than for the off-nuclear regions or the SINGS H II galaxies. Panel (c), for example, shows that half of the RSA Seyfert nuclei have $L(8.6 \mu\text{m})/L(11.3 \mu\text{m})$ ratios < 0.5 , whereas for the H II galaxies, half have ratios < 0.75 . The remaining three panels show that the ratios among the 6.2, 7.7, and 8.6 μm features show no significant differences between any of the samples.

3.1. Aromatic Feature Ratio Distributions

In Figure 4, we show the distribution of aromatic feature ratios for the 35 RSA Seyfert nuclei and 21 off-nuclear regions, as well as for 27/59 SINGS galaxies from Smith et al. (2007a) that have H II nuclear classifications (i.e., those that are not Seyferts or LINERs). We find that the $L(6.2 \mu\text{m})/L(11.3 \mu\text{m})$, $L(7.7 \mu\text{m})/L(11.3 \mu\text{m})$, and $L(8.6 \mu\text{m})/L(11.3 \mu\text{m})$ ratios are systematically lower for the Seyfert nuclei than for the off-nuclear regions or the SINGS H II galaxies. These differences are all statistically significant with $p \leq 0.003$ based on the two-sample Kolmogorov–Smirnov (K-S) test (see Table 3), a non-parametric test that considers the maximum deviation between two cumulative distribution functions (Press et al. 1992; Wall & Jenkins 2003). On the other hand, there are no significant differences between these feature ratios for the off-nuclear regions and the SINGS H II galaxies, so the feature strengths in regions of star formation are consistent with being drawn from the same parent distribution. Furthermore, the ratios among the 6.2, 7.7, and 8.6 μm features show no significant differences between any of the samples.

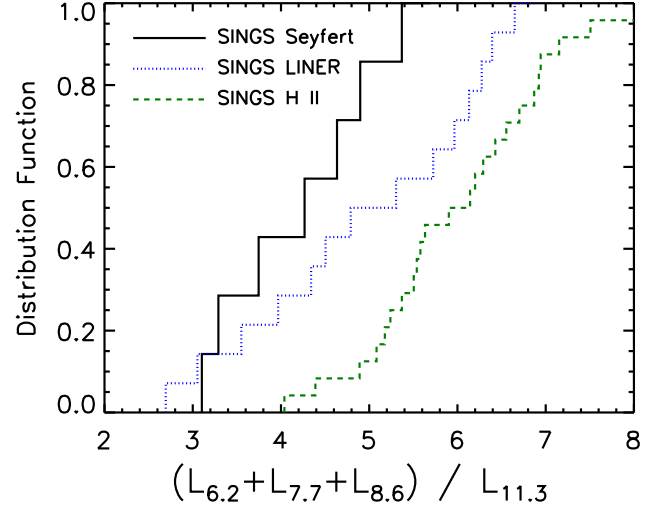


FIG. 5.— The cumulative distribution of the ratio of 6.2, 7.7, and 8.6 μm features to the 11.3 μm feature for SINGS galaxies with Seyfert, LINER, and H II optical classifications. This illustrates the result found by Smith et al. (2007a) that the Seyferts and LINERs have ratios that are significantly lower than the H II galaxies. The apparent difference between SINGS Seyferts and LINERs is not statistically significant.

Smith et al. (2007a) noted that the LINERs and Seyferts in the SINGS sample were offset towards lower $L(7.7 \mu\text{m})/L(11.3 \mu\text{m})$ ratios when compared to the H II galaxies. We illustrate this result graphically in Figure 5, which shows the distribution functions of the ratio of 6.2, 7.7, and 8.6 μm features to the 11.3 μm feature for galaxies with Seyfert, LINER, and H II optical classifications. Both Seyferts ($p = 2 \times 10^{-3}$) and LINERs ($p = 0.04$) have ratios that are significantly lower than the H II galaxies. While the SINGS Seyferts have somewhat lower ratios than the LINERs, this difference is not statistically significant, and neither sample is statistically distinguishable from the RSA Seyferts.

3.2. Trends with H_2 emission

Inspection of Figure 2 reveals that several Seyferts with small $L(7.7 \mu\text{m})/L(11.3 \mu\text{m})$ aromatic feature ratios also exhibit a strong H_2 S(3) rotational line at 9.67 μm (e.g., NGC4501, NGC5194.) To investigate this behavior, we plot the strength of the H_2 S(3) line, normalized to the strength of the aromatic features, as a function of the $L(7.7 \mu\text{m})/L(11.3 \mu\text{m})$ ratio in Figure 6. We find a strong anti-correlation in this plot such that sources with the smallest $L(7.7 \mu\text{m})/L(11.3 \mu\text{m})$ ratios also have the strongest H_2 emission. The Spearman's ρ rank correlation coefficient is -0.78 with a probability $p = 3 \times 10^{-8}$ of no correlation, while Kendall's τ is -0.62 with $p = 1 \times 10^{-7}$; these non-parametric tests consider the agreement between the ranks of quantities in pairs of measurements (Press et al. 1992; Wall & Jenkins 2003), with coefficient values ranging from -1 (perfect disagreement) to 1 (perfect agreement). Roussel et al. (2007) found that H_2 rotational lines scale tightly with the aromatic features for SINGS H II galaxies, but that Seyferts and LINERs often exhibit excess H_2 emission, which they attribute to shocks. We explore the hypoth-

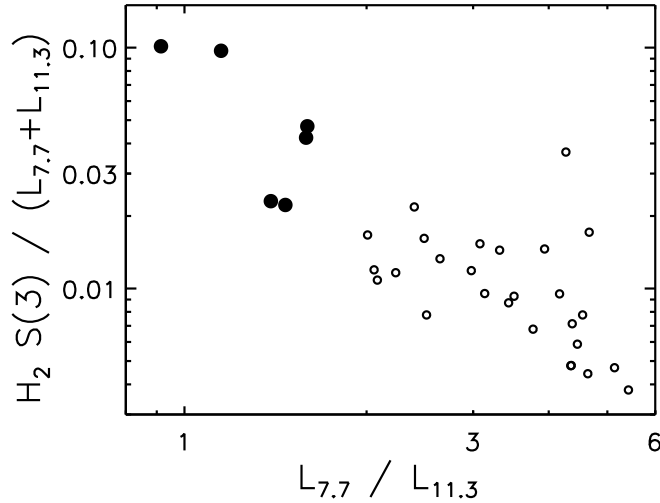


FIG. 6.— The relationship between the strength of the H₂ S(3) rotational line, normalized to the strength of the aromatic features, and the L(7.7 μm)/L(11.3 μm) ratio for RSA Seyfert nuclei. The sources with small L(7.7 μm)/L(11.3 μm) ratios also exhibit strong H₂ emission. The most extreme sources with L(7.7 μm)/L(11.3 μm) < 1.6 are highlighted with filled circles.

esis that shocks cause both the excess H₂ emission and the anomalous aromatic ratios for AGNs in Section 4.4.

Among the sources excluded from the above analysis due to a lack of 6.2, 7.7, or 8.6 μm aromatic feature detections, there are a significant number with clearly detected 11.3 μm features and H₂ S(3) lines. In Figure 7, we show the nuclear spectra for a dozen of these sources, sorted by the equivalent width of the 11.3 μm feature. These spectra exhibit the small L(7.7 μm)/L(11.3 μm) ratios and strong H₂ S(3) lines characteristic of sources in the top-left of Figure 6. Due to uncertainties associated with estimating the strength of weak, broad features and determining robust upper limits (e.g., proper continuum placement), we do not include any of these sources in our subsequent analysis. However, their behavior is consistent with that in Figure 6 and supports the reality of the trend between aromatic feature characteristics and H₂ line strength.

3.3. Evidence for extinction of aromatic features

The sources with the largest L(7.7 μm)/L(11.3 μm) ratios, NGC4945 and NGC3079, also have the strongest silicate absorption features. This suggests that the 11.3 μm feature is being significantly attenuated, consistent with previous results for starburst and luminous infrared galaxies (e.g., Brandl et al. 2006; Pereira-Santaella et al. 2010), and implies that a significant fraction of the silicate-absorbing material is extended relative to the regions that produce the aromatic features. Although the aromatic feature measurements in PAHFIT are corrected for extinction, in cases as extreme as these two galaxies the resulting feature strengths are highly uncertain. For all other galaxies in our sample, the inferred extinctions are < 50% for all features.

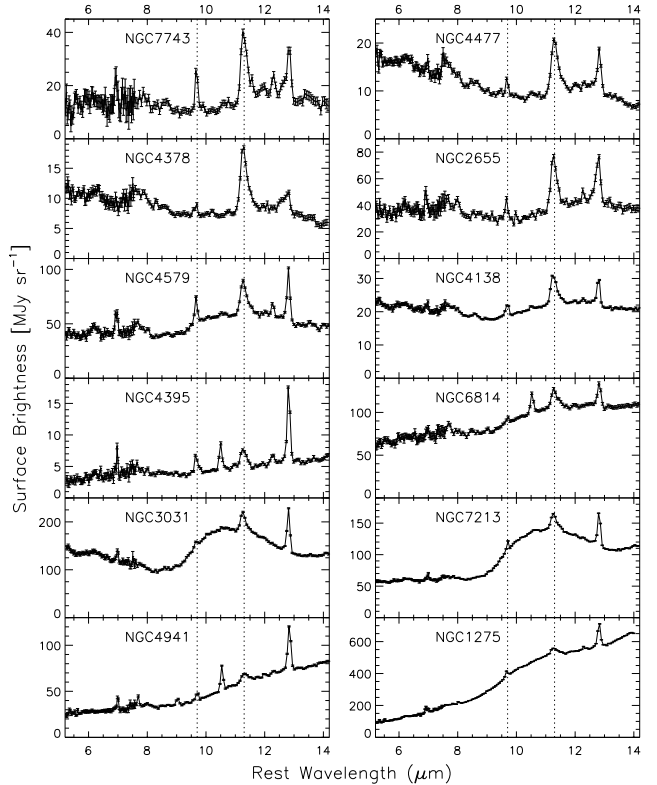


FIG. 7.— Nuclear spectra for 12 additional RSA Seyfert nuclei that exhibit small L(7.7 μm)/L(11.3 μm) ratios and strong H₂ S(3) lines, but were excluded from the sample due to a lack of 6.2, 7.7, or 8.6 μm aromatic feature detections. The spectra are sorted from top to bottom by the equivalent width of the 11.3 μm aromatic feature. The wavelengths of the 9.67 μm H₂ S(3) line and the 11.3 μm aromatic feature are marked by dotted lines.

4. DISCUSSION

The result that Seyfert galaxies exhibit weak 6.2, 7.7, and 8.6 μm aromatic features relative to the 11.3 μm feature could be explained by radiative or mechanical processing of the molecular carriers by the active nucleus. Here we explore the relevant physical and chemical effects that could modify the observed feature strengths.

4.1. Ionization Balance

Previous experimental (e.g., Szczepanski & Vala 1993; Hudgins & Allamandola 1995) and theoretical (e.g., DeFrees et al. 1993; Langhoff 1996) work on PAHs has shown that the C–C stretching modes that produce the 6.2 and 7.7 μm features, as well as the C–H in-plane bending modes that produce the 8.6 μm feature, are more efficiently excited in ionized molecules. The ratios of these features to the 11.3 μm feature, which is produced by C–H out-of-plane bending modes, are lower for neutral molecules (see Figure 1 of Allamandola et al. 1999). The fraction of ionized aromatic molecules is set by the balance between ionization and recombination, which depends on the UV radiation field density (G_0), the gas temperature (T), and the electron density (n_e) according to $G_0 T^{1/2}/n_e$ (Bakes & Tielens 1994).

Galliano et al. (2008) argued that the variations in aromatic feature ratios for a heterogeneous sample of 50

objects (including Galactic regions, Magellanic H II regions, and galaxies, as well as spatially resolved regions within seven of those objects) are controlled by this ionization balance. Similar to our results, they found that the relative strengths of 6.2, 7.7, and 8.6 μm features showed little variation, while the ratios between these features and the 11.3 μm feature varied by an order of magnitude. This hypothesis is also supported by observations of Galactic reflection nebulae by Joblin et al. (1996) and Bregman & Temi (2005), who found decreasing $L(8.6 \mu\text{m})/L(11.3 \mu\text{m})$ and $L(7.7 \mu\text{m})/L(11.3 \mu\text{m})$ ratios as a function of distance from the ionizing source, consistent with an increasing neutral fraction.

To compare with model expectations for ionized and neutral aromatic molecules, we plot $L(11.3 \mu\text{m})/L(7.7 \mu\text{m})$ v. $L(6.2 \mu\text{m})/L(7.7 \mu\text{m})$ for the Seyfert nuclei, off-nuclear sources, and SINGS H II galaxies in Figure 8. This can be compared with Figure 16 of Draine & Li (2001) and Figure 5 of O’Dowd et al. (2009), although we use a condensed plot range. We find that a number of Seyferts lie beyond the range of model predictions, even for completely neutral aromatic molecules; these are the 6/35 Seyferts with $L(11.3 \mu\text{m})/L(7.7 \mu\text{m}) > 0.6$: NGC5194, NGC4501, NGC4639, NGC1433, NGC2639, and NGC5005. While such $L(11.3 \mu\text{m})/L(7.7 \mu\text{m})$ ratios could be produced by large (> 200 C atoms) neutral molecules, they would be expected to have $L(6.2 \mu\text{m})/L(7.7 \mu\text{m}) < 0.25$, which is inconsistent with the data. Similar extreme aromatic band strengths were observed by Reach et al. (2000) for the quiescent molecular cloud SMC B1 No. 1, and Li & Draine (2002) were unable to reproduce the observed band ratios even with completely neutral grains.

The above comparison is for a single Milky Way-based model, and laboratory studies have found larger $L(11.3 \mu\text{m})/L(7.7 \mu\text{m})$ ratios for neutral PAHs, but it does illustrate the difficulty in explaining our results for Seyfert galaxies in terms of a low ionized fraction. Furthermore, under the assumption that aromatic features are produced by star formation (see Section 4.5), the temperatures and densities of the aromatic-emitting regions should be typical of PDRs, whereas the UV radiation field would likely be enhanced by the AGN. This implies that the ionized fraction would be higher, not lower. Thus, ionization balance arguments appear unable to explain the behavior of the aromatic features around AGNs.

4.2. Grain Size

Smaller aromatic molecules contribute preferentially to the shorter-wavelength features (e.g., Schutte et al. 1993), but they are subject to photodestruction by the UV radiation field and collisional destruction by shocks. Based on laboratory studies, Jochims et al. (1994) found a critical size of 30–40 C atoms, below which PAHs would mainly be photodissociated, while Allain et al. (1996) suggested a larger critical value of 50 C atoms based on their models. Le Page et al. (2003) agreed that small PAHs with 15–20 C atoms or fewer would be destroyed in most environments, but their models indicated that PAHs in the 20–30 C atom range may survive, albeit with most of their peripheral H atoms stripped away, while larger PAHs would survive with their H atoms in-

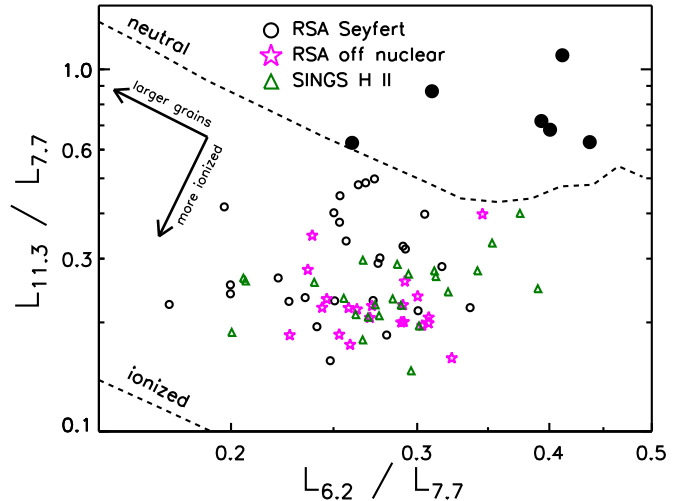


FIG. 8.— The relative strengths of the 6.2, 7.7, and 11.3 μm features for RSA Seyfert nuclei, off-nuclear regions, and SINGS H II galaxies compared with model predictions from Draine & Li (2001) for neutral and ionized PAHs. The dashed lines correspond to predictions for completely neutral and completely ionized molecules; the permitted region of the diagram is bounded by these two lines. The arrows illustrate the effects of increasing grain size and increasing ionization on the aromatic feature ratios. The Seyferts highlighted as filled circles in Figure 6 all lie beyond the range of model predictions, even for completely neutral molecules.

tact. Micelotta et al. (2010a) found that PAHs with 50 C atoms would not survive in shocks with velocities greater than 100 km s^{-1} , while PAHs with 200 C atoms would be destroyed by shocks with velocities above 125 km s^{-1} .

Destruction of the smallest molecules is expected to result in the 6.2 and 7.7 μm features being suppressed relative to the 11.3 μm feature, as well as the 6.2 μm feature being suppressed relative to the 7.7 μm feature (e.g., Draine & Li 2001; Galliano et al. 2008). The former effect is clearly seen in Figure 4, but the latter is not. Thus, the hypothesis that small-grain destruction can explain the observed ratios is only tenable if the molecules that produce the 6.2, 7.7, and 8.6 μm features are destroyed with similar efficiency, which is inconsistent with existing models.

4.3. Hydrogenation and Molecular Structure

The level of hydrogenation of the aromatic molecules will affect the number of C–H bonds and therefore the relative strength of the C–H and C–C vibrational modes. An increase in the C–H/C–C ratio was proposed by Reach et al. (2000) to explain the large $L(11.3 \mu\text{m})/L(7.7 \mu\text{m})$ ratio observed in SMC B1 No. 1, although Draine & Li (2001) and Li & Draine (2002) point out that PAHs with > 30 C atoms are already expected to be fully hydrogenated. Some range in C–H/C–C ratios, even for fully hydrogenated molecules, is facilitated by the structure of the C skeleton, which can be compact with more C–C bonds or open with more C–H bonds (e.g., pericondensed PAHs v. cata-condensed PAHs, Tielens 2005). The structure also affects the number of adjacent C–H groups per aromatic ring, and therefore the relative strengths of the 11.3 μm feature, which is produced by solo C–H bonds, and the

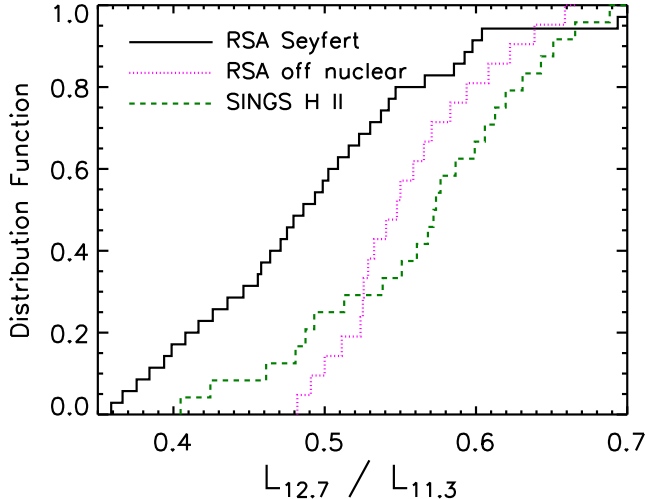


FIG. 9.— The cumulative distribution of $L(12.7 \mu\text{m})/L(11.3 \mu\text{m})$ ratios for RSA Seyfert nuclei, off-nuclear regions, and SINGS H II galaxies. The result that Seyfert nuclei exhibit significantly smaller ratios suggests aromatic molecules that have fewer adjacent C–H groups.

$12.7 \mu\text{m}$ feature, which is produced by C–H multiplets (e.g., Hony et al. 2001). For example, based on the large $L(12.7 \mu\text{m})/L(11.3 \mu\text{m})$ ratio for SMC B1 No. 1, Vermeij et al. (2002) argued for a compact structure with a higher incidence of C–H multiplets.

To investigate such behavior, we plot the $L(12.7 \mu\text{m})/L(11.3 \mu\text{m})$ ratios for Seyfert nuclei, off-nuclear regions, and SINGS H II galaxies in Figure 9. The Seyfert nuclei exhibit significantly smaller ratios ($p \leq 0.001$), while the ratios for off-nuclear regions and SINGS H II galaxies are not distinguishable. This implies that the aromatic molecules in Seyfert nuclei may have fewer C–H multiplets. Thus a scenario where AGN processing or environment results in open, uneven molecular structures with higher C–H/C–C ratios and fewer adjacent C–H groups could qualitatively explain the observed 6–13 μm aromatic spectra.

4.4. The role of AGN-driven shocks

As presented in Section 3.2 and Figure 6, the Seyfert galaxies with the smallest $L(7.7 \mu\text{m})/L(11.3 \mu\text{m})$ aromatic feature ratios also exhibit the strongest $\text{H}_2 \text{ S}(3)$ emission, which probes hot molecular gas (upper level temperature 2500 K). The incidence of this excess H_2 emission does not scale with AGN luminosity, indicating that shock excitation is more important than X-ray heating (e.g., Roussel et al. 2007). A connection between shock-heated, H_2 -emitting gas and small $L(7.7 \mu\text{m})/L(11.3 \mu\text{m})$ ratios was found by Ogle et al. (2007) for the radio galaxy 3C 326 and by Guillard et al. (2010) for Stephan’s Quintet, a compact group of interacting galaxies exhibiting a large-scale shock (e.g., Appleton et al. 2006; Cluver et al. 2010). Similarly, Kaneda et al. (2008) found strong H_2 emission and small $L(7.7 \mu\text{m})/L(11.3 \mu\text{m})$ ratios in a sample of local elliptical galaxies, many of which host low-luminosity AGNs. More recently, Vega et al. (2010) affirmed this

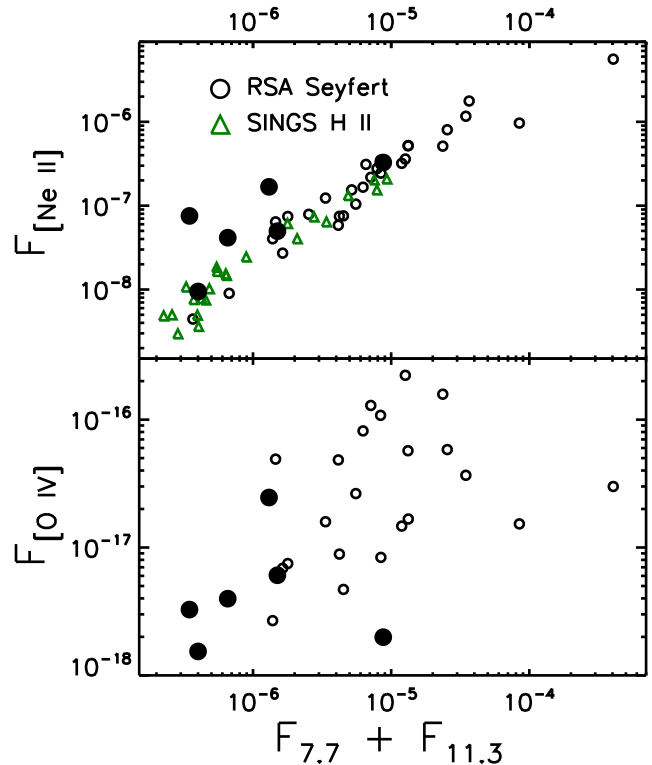


FIG. 10.— The relationship between the aromatic features and the [Ne II] and [O IV] emission lines. The filled circles correspond to the RSA Seyferts defined in Figure 6 that have the smallest $L(7.7 \mu\text{m})/L(11.3 \mu\text{m})$ ratios. The strong correlation with [Ne II], which traces star formation, and the weak correlation with [O IV], which traces AGN activity, implies that the aromatic features are primarily associated with star formation. Most of the Seyfert nuclei lie on the relationship between aromatic feature and [Ne II] emission for H II galaxies; the only outliers are among the sources highlighted with filled circles, which have extreme aromatic feature ratios (see Figures 6 and 8). The aromatic feature and [Ne II] emission values are in surface brightness units ($\text{W m}^{-2} \text{sr}^{-1}$), while the [O IV] values, taken from Diamond-Stanic et al. (2009), are in flux units (W m^{-2}).

result for a sample of four early-type galaxies classified as LINERs, and they argued that shock processing of aromatic molecules may be responsible for the observed behavior. As discussed above, the Seyferts and LINERs in the SINGS sample also exhibit smaller $L(7.7 \mu\text{m})/L(11.3 \mu\text{m})$ ratios (Smith et al. 2007a) and stronger H_2 emission (Roussel et al. 2007) than do the H II galaxies.

Shocks are expected to have profound impacts on interstellar dust via shattering in grain-grain collisions and sputtering in ion-grain collisions (e.g., Jones et al. 1994, 1996). Aromatic features are nonetheless observed in the shocked environments of supernova remnants (e.g., Tappe et al. 2006; Reach et al. 2006) and galactic winds (e.g., Tacconi-Garman et al. 2005; Engelbracht et al. 2006). The observed emission may come from entrained clumps that are not fully exposed to the shock or the hot, post-shock gas (Micelotta et al. 2010a,b). Micelotta et al. (2010a) study the processing of small

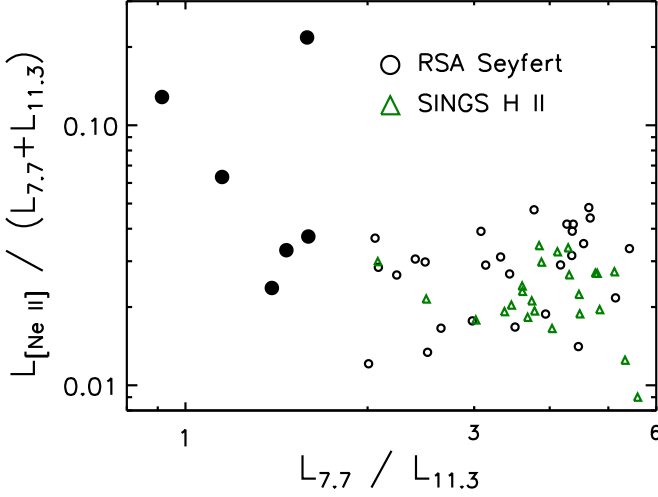


FIG. 11.— The relationship between aromatic feature and [Ne II] emission as a function of the $L(7.7 \mu\text{m})/L(11.3 \mu\text{m})$ ratio. The filled circles correspond to the RSA Seyferts defined in Figure 6 that have the smallest $L(7.7 \mu\text{m})/L(11.3 \mu\text{m})$ ratios. This confirms that the sources with suppressed aromatic features, relative to [Ne II], have the smallest $L(7.7 \mu\text{m})/L(11.3 \mu\text{m})$ ratios.

carbon grains ($N_C \leq 200$, corresponding to aromatic molecules) by interstellar shocks and find that their molecular structure is severely denatured for shock velocities of $75\text{--}100 \text{ km s}^{-1}$ and they are completely destroyed when $v \geq 125 \text{ km s}^{-1}$. The effect of this shock processing on the observed aromatic feature ratios is not known. A possibility that could explain the association of modified aromatic feature ratios with strong H_2 emission is that shocks may leave open, uneven structures in the surviving aromatic molecules. We note that AGN-driven shocks, if responsible for the observed behavior, do not strongly suppress the $11.3 \mu\text{m}$ feature (see Section 4.6).

4.5. Could the aromatic features be excited by the AGN?

Smith et al. (2007a) speculated that the AGNs could directly excite aromatic emission. If this were the case, SFRs estimated from aromatic features would be overestimated due to this AGN contribution. To investigate the relationship between star formation rate, AGN luminosity, and aromatic feature strength, we plot the fluxes of the [Ne II] and [O IV] emission lines versus those of the $7.7 \mu\text{m}$ and $11.3 \mu\text{m}$ aromatic features in Figure 10. The [Ne II] line has an ionization potential of 21 eV and is a reasonable tracer of the SFR (e.g., Ho & Keto 2007), while the [O IV] line has an ionization potential of 55 eV and traces the AGN intrinsic luminosity (e.g., Meléndez et al. 2008; Diamond-Stanic et al. 2009; Rigby et al. 2009). Figure 10 shows the strong correlation between [Ne II] and aromatic feature strength for RSA Seyferts (Spearman’s $\rho = 0.93$), which matches the relationship for SINGS H II galaxies, and it shows the weak correspondence between [O IV] and aromatic feature strength (Spearman’s $\rho = 0.39$). This confirms that the aromatic features are primarily tracing star formation activity.

The Seyferts that are outliers in the [Ne II]–aromatic

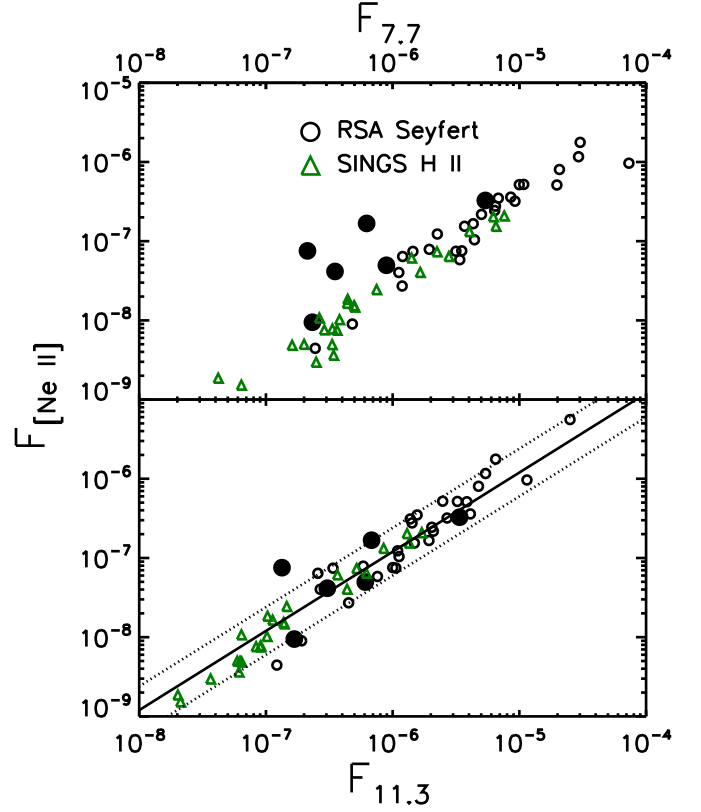


FIG. 12.— The relationship between [Ne II] emission and the 7.7 and $11.3 \mu\text{m}$ aromatic features. The filled circles correspond to the RSA Seyferts defined in Figure 6 that have the smallest $L(7.7 \mu\text{m})/L(11.3 \mu\text{m})$ ratios. While the $7.7 \mu\text{m}$ feature can be strongly suppressed, the $11.3 \mu\text{m}$ feature is still a robust tracer of the SFR. The solid line in the bottom panel corresponds to the median ratio $L[\text{Ne II}]/L_{11.3} = 0.12$, and the dotted lines correspond to factors of two above and below this median value. Scatter in this ratio is expected because [Ne II] traces somewhat younger stellar populations than do the aromatic features. All values are in surface brightness units ($\text{W m}^{-2} \text{ sr}^{-1}$).

feature relationship have weak aromatic features, and we show in Figure 11 that these correspond to the sources with the smallest $L(7.7 \mu\text{m})/L(11.3 \mu\text{m})$ ratios. There are no examples with stronger aromatic features as might be expected if the AGN were exciting additional emission. The three obvious outliers, NGC2639, NGC4501, and NGC5194, all have $[\text{O IV}]/[\text{Ne II}] < 0.25$, implying that the AGN contribution to [Ne II] is $< 10\%$ (e.g., Sturm et al. 2002). We note that the incidence of modified aromatic spectra does not show a dependence on AGN luminosity, confirming the results of Baum et al. (2010), who found no correlation between the $L(6.2 \mu\text{m})/L(11.3 \mu\text{m})$ ratio and [Ne V] luminosity.

4.6. Use of Aromatic Features to Determine SFRs

Several studies (e.g., Schweitzer et al. 2006; Lutz et al. 2008; Shi et al. 2009) have used the 6.2 and $7.7 \mu\text{m}$ aromatic features to measure the SFRs in AGN host galaxies. The result that some AGNs exhibit suppressed short-wavelength aromatic features (e.g., the outliers in Figure 11) suggests that such SFR measurements may be underestimated. To determine whether the $11.3 \mu\text{m}$ feature

is robust to such effects, we plot separately the relationships between [Ne II] and the 7.7 and 11.3 μm features in Figure 12. We find that almost all of the RSA Seyferts, including those with anomalously high $L_{[\text{Ne II}]} / L_{7.7}$ values, are within a factor of two of the median value $L_{[\text{Ne II}]} / L_{11.3} = 0.12$. Scatter in this ratio is expected as a function of the age of the stellar population because 21 eV photons from young stars (< 10 Myr) are required to produce [Ne II], while somewhat older stars can produce 6–13.6 eV UV photons that excite aromatic emission (e.g., Peeters et al. 2004; Díaz-Santos et al. 2010; Pereira-Santaella et al. 2010). Silicate absorption will tend to increase the observed ratio, but this is only a significant effect for sources like NGC4945 and NGC3079 (see Section 3.3). While SFR estimates based on the 11.3 μm feature are still subject to the uncertainties that apply to H II galaxies (e.g., Smith et al. 2007a), such measurements for AGN hosts appear to be robust to the effects of AGN- and shock-processing of aromatic molecules.

5. CONCLUSIONS

We have shown that the relative strengths of the mid-IR aromatic features for Seyfert galaxies differ significantly from those for star-forming galaxies, with the 6.2, 7.7, and 8.6 μm features being suppressed relative to the 11.3 μm feature in Seyferts. The sources with the smallest $L(7.7 \mu\text{m}) / L(11.3 \mu\text{m})$ aromatic feature ratios also exhibit the strongest H₂ S(3) rotational lines, which likely trace shocked gas (see Figure 6). We explore the relevant physical and chemical effects that could produce the observed aromatic spectra. An enhanced fraction of neutral aromatic molecules could produce qualitatively similar behavior, but the observed ratios lie be-

yond model predictions for completely neutral molecules and the presence of an AGN would be expected to increase the level of ionization rather than reduce it. Destruction of the smallest aromatic molecules could explain the suppression of shorter wavelength features, but the expected variations in the relative strengths of the 6.2, 7.7, and 8.6 μm features are not seen. A modification of the molecular structure that enhances the C–H/C–C ratio could reproduce the observed behavior, and an open C skeleton with fewer adjacent C–H groups would furthermore explain the reduced strength of the 12.7 μm feature. Given the connection between strong H₂ emission and modified aromatic ratios, we speculate that shock processing could produce such structures. Finally, we show that the aromatic features correlate well with [Ne II] (i.e., star formation) but not with [O IV] (i.e., AGN luminosity), indicating that AGN excitation of aromatic emission is not significant and that aromatic-based estimates of the SFR are generally reasonable. There are a few outliers with strong H₂ emission, small $L(7.7 \mu\text{m}) / L(11.3 \mu\text{m})$ ratios, and small aromatic/[Ne II] ratios, but for these sources the 11.3 μm feature is still a reasonably robust tracer of the SFR.

We acknowledge useful discussions with and assistance from Anthony Jones, Yong Shi, Amelia Stutz, Alexander Tielens, Jonathan Trump, and Gregory Walth. We thank the anonymous referee for helpful suggestions that have improved the manuscript. This work was supported by contract 1255094 from Caltech/JPL to the University of Arizona.

Facilities: Spitzer

REFERENCES

- Allain, T., Leach, S., & Sedlmayr, E. 1996, *A&A*, 305, 602
Allamandola, L. J., Tielens, A. G. G. M., & Barker, J. R. 1985, *ApJ*, 290, L25
Allamandola, L. J., Tielens, A. G. G. M., & Barker, J. R. 1989, *ApJS*, 71, 733
Allamandola, L. J., Hudgins, D. M., & Sandford, S. A. 1999, *ApJ*, 511, L115
Appleton, P. N., et al. 2006, *ApJ*, 639, L51
Bakes, E. L. O., & Tielens, A. G. G. M. 1994, *ApJ*, 427, 822
Bakes, E. L. O., Tielens, A. G. G. M., & Bauschlicher, C. W., Jr. 2001, *ApJ*, 556, 501
Baum, S. A., et al. 2010, *ApJ*, 710, 289
Brandl, B. R., et al. 2006, *ApJ*, 653, 1129
Bregman, J., & Temi, P. 2005, *ApJ*, 621, 831
Calzetti, D., et al. 2007, *ApJ*, 666, 870
Cluver, M. E., et al. 2010, *ApJ*, 710, 248
Diamond-Stanic, A. M., Rieke, G. H., & Rigby, J. R. 2009, *ApJ*, 698, 623
Díaz-Santos, T., Alonso-Herrero, A., Colina, L., Packham, C., Levenson, N. A., Pereira-Santaella, M., Roche, P. F., & Telesco, C. M. 2010, *ApJ*, 711, 328
DeFrees, D. J., Miller, M. D., Talbi, D., Pauzat, F., & Ellinger, Y. 1993, *ApJ*, 408, 530
Draine, B. T., & Li, A. 2001, *ApJ*, 551, 807
Duley, W. W., & Williams, D. A. 1981, *MNRAS*, 196, 269
Engelbracht, C. W., et al. 2006, *ApJ*, 642, L127
Galliano, F., Madden, S. C., Tielens, A. G. G. M., Peeters, E., & Jones, A. P. 2008, *ApJ*, 679, 310
Genzel, R., et al. 1998, *ApJ*, 498, 579
Guillard, P., Boulanger, F., Cluver, M. E., Appleton, P. N., Pineau des Forets, G., & Ogle, P. 2010, *arXiv:1004.0677*
Ho, L. C., Filippenko, A. V., & Sargent, W. L. W. 1997, *ApJS*, 112, 315
Ho, L. C., & Keto, E. 2007, *ApJ*, 658, 314
Hony, S., Van Kerckhoven, C., Peeters, E., Tielens, A. G. G. M., Hudgins, D. M., & Allamandola, L. J. 2001, *A&A*, 370, 1030
Houck, J. R., et al. 2004, *ApJS*, 154, 18
Hudgins, D. M., & Allamandola, L. J. 1995, *J. Phys. Chem.*, 99, 3033
Joblin, C., Tielens, A. G. G. M., Geballe, T. R., & Wooden, D. H. 1996, *ApJ*, 460, L119
Jochims, H. W., Ruhl, E., Baumgartel, H., Tobita, S., & Leach, S. 1994, *ApJ*, 420, 307
Jones, A. P., Tielens, A. G. G. M., Hollenbach, D. J., & McKee, C. F. 1994, *ApJ*, 433, 797
Jones, A. P., Tielens, A. G. G. M., & Hollenbach, D. J. 1996, *ApJ*, 469, 740
Kaneda, H., Onaka, T., Sakon, I., Kitayama, T., Okada, Y., & Suzuki, T. 2008, *ApJ*, 684, 270
Kennicutt, R. C., Jr., et al. 2003, *PASP*, 115, 928
Langhoff, S. R. 1996, *J. Phys. Chem.*, 100, 2819
Leger, A., & Puget, J. L. 1984, *A&A*, 137, L5
Le Page, V., Snow, T. P., & Bierbaum, V. M. 2003, *ApJ*, 584, 316
Li, A., & Draine, B. T. 2001, *ApJ*, 554, 778
Li, A., & Draine, B. T. 2002, *ApJ*, 576, 762
Lu, N., et al. 2003, *ApJ*, 588, 199
Lutz, D., et al. 2008, *ApJ*, 684, 853
Maiolino, R., & Rieke, G. H. 1995, *ApJ*, 454, 95
Meléndez, M., et al. 2008, *ApJ*, 682, 94
Micelotta, E. R., Jones, A. P., & Tielens, A. G. G. M. 2010, *A&A*, 510, A36
Micelotta, E. R., Jones, A. P., & Tielens, A. G. G. M. 2010, *A&A*, 510, A37
O’Dowd, M. J., et al. 2009, *ApJ*, 705, 885
Ogle, P., Antonucci, R., Appleton, P. N., & Whysong, D. 2007, *ApJ*, 668, 699
Peeters, E., Spoon, H. W. W., & Tielens, A. G. G. M. 2004, *ApJ*, 613, 986
Pereira-Santaella, M., Alonso-Herrero, A., Rieke, G. H., Colina, L., Díaz-Santos, T., Smith, J. D. T., Perez-Gonzalez, P. G., & Engelbracht, C. W. 2010, *arXiv:1004.1364*
Povich, M. S., et al. 2007, *ApJ*, 660, 346

- Press, W. H., Teukolsky, S. A., Vetterling, W. T., & Flannery, B. P. 1992, *Numerical Recipes: The Art of Scientific Computing*, 2nd ed. (Cambridge: Cambridge Univ. Press)
- Reach, W. T., Boulanger, F., Contursi, A., & Lequeux, J. 2000, *A&A*, 361, 895
- Reach, W. T., et al. 2006, *AJ*, 131, 1479
- Rieke, G. H., Alonso-Herrero, A., Weiner, B. J., Pérez-González, P. G., Blaylock, M., Donley, J. L., & Marcillac, D. 2009, *ApJ*, 692, 556
- Rigby, J. R., Diamond-Stanic, A. M., & Aniano, G. 2009, *ApJ*, 700, 1878
- Roche, P. F., Aitken, D. K., Smith, C. H., & Ward, M. J. 1991, *MNRAS*, 248, 606
- Roussel, H., et al. 2007, *ApJ*, 669, 959
- Roseboom, I. G., Oliver, S., & Farrah, D. 2009, *ApJ*, 699, L1
- Sandage, A., & Tammann, G. A. 1987, *A Revised Shapley–Ames Catalog of Bright Galaxies* (2nd ed. Washington, DC: Carnegie Institution of Washington)
- Schutte, W. A., Tielens, A. G. G. M., & Allamandola, L. J. 1993, *ApJ*, 415, 397
- Schweitzer, M., et al. 2006, *ApJ*, 649, 79
- Shi, Y., et al. 2007, *ApJ*, 669, 841
- Shi, Y., Rieke, G. H., Ogle, P., Jiang, L., & Diamond-Stanic, A. M. 2009, *ApJ*, 703, 1107
- Smith, J. D. T., et al. 2007, *ApJ*, 656, 770
- Smith, J. D. T., et al. 2007, *PASP*, 119, 1133
- Sturm, E., Lutz, D., Verma, A., Netzer, H., Sternberg, A., Moorwood, A. F. M., Oliva, E., & Genzel, R. 2002, *A&A*, 393, 821
- Szczepanski, J., & Vala, M. 1993, *ApJ*, 414, 646
- Tacconi-Garman, L. E., Sturm, E., Lehnert, M., Lutz, D., Davies, R. I., & Moorwood, A. F. M. 2005, *A&A*, 432, 91
- Tappe, A., Rho, J., & Reach, W. T. 2006, *ApJ*, 653, 267
- Tielens, A. G. G. M. 2005, *The Physics and Chemistry of the Interstellar Medium* (Cambridge: Cambridge Univ. Press)
- Tielens, A. G. G. M. 2008, *ARA&A*, 46, 289
- Vega, O., et al. 2010, *ApJ*, in press, arXiv:1008.0009
- Vermeij, R., Peeters, E., Tielens, A. G. G. M., & van der Hulst, J. M. 2002, *A&A*, 382, 1042
- Voit, G. M. 1992, *MNRAS*, 258, 841
- Wall, J. V. & Jenkins, C. R. 2003, *Practical Statistics for Astronomers* (Cambridge: Cambridge Univ. Press)
- Werner, M. W., et al. 2004, *ApJS*, 154, 1

TABLE 1
NUCLEAR MEASUREMENTS

NAME	6.2 μm	7.7 μm^{a}	8.6 μm	11.3 μm^{b}	12.7 μm^{c}	[Ne II]	H ₂ S(3)
IC3639	1.15 \pm 0.05e-06	5.19 \pm 0.79e-06	3.41 \pm 0.54e-07	1.38 \pm 0.05e-06	4.94 \pm 0.54e-07	3.11 \pm 0.05e-07	4.45 \pm 0.79e-08
NGC1058	1.47 \pm 0.10e-07	4.81 \pm 0.64e-07	9.52 \pm 0.69e-08	1.91 \pm 0.06e-07	9.12 \pm 0.88e-08	9.00 \pm 1.09e-09	5.22 \pm 1.28e-09
NGC1097	9.24 \pm 0.31e-07	3.69 \pm 0.19e-06	6.90 \pm 0.22e-07	1.48 \pm 0.03e-06	8.07 \pm 0.21e-07	1.54 \pm 0.02e-07	8.36 \pm 0.68e-08
NGC1241	5.38 \pm 0.83e-07	1.95 \pm 0.44e-06	3.50 \pm 0.44e-07	5.86 \pm 0.71e-07	2.67 \pm 0.35e-07	7.89 \pm 0.48e-08	3.65 \pm 1.61e-08
NGC1365	4.77 \pm 0.07e-06	1.98 \pm 0.05e-05	3.10 \pm 0.05e-06	3.85 \pm 0.04e-06	3.00 \pm 0.06e-06	5.12 \pm 0.05e-07	1.11 \pm 0.07e-07
NGC1433	3.58 \pm 0.25e-07	8.93 \pm 1.79e-07	2.50 \pm 0.18e-07	6.08 \pm 0.15e-07	2.66 \pm 0.23e-07	4.96 \pm 0.21e-08	3.34 \pm 0.62e-08
NGC1566	8.12 \pm 0.25e-07	3.16 \pm 0.14e-06	5.14 \pm 0.20e-07	1.06 \pm 0.01e-06	4.87 \pm 0.18e-07	7.46 \pm 0.20e-08	5.01 \pm 0.32e-08
NGC2273	2.54 \pm 0.03e-06	9.23 \pm 0.14e-06	1.45 \pm 0.02e-06	2.69 \pm 0.03e-06	1.08 \pm 0.02e-06	3.20 \pm 0.03e-07	1.04 \pm 0.04e-07
NGC2639	9.29 \pm 0.97e-08	2.13 \pm 0.61e-07	4.19 \pm 0.66e-08	1.34 \pm 0.05e-07	8.02 \pm 0.71e-08	7.55 \pm 0.09e-08	1.47 \pm 0.13e-08
NGC2992	1.55 \pm 0.05e-06	6.82 \pm 0.35e-06	8.24 \pm 0.36e-07	1.56 \pm 0.03e-06	7.80 \pm 0.43e-07	3.49 \pm 0.04e-07	5.99 \pm 0.52e-08
NGC3079	1.82 \pm 0.03e-05	7.32 \pm 0.08e-05	1.19 \pm 0.03e-05	1.15 \pm 0.03e-05	6.68 \pm 0.07e-06	9.66 \pm 0.10e-07	5.04 \pm 0.26e-07
NGC3185	1.11 \pm 0.05e-06	3.51 \pm 0.26e-06	6.99 \pm 0.40e-07	1.00 \pm 0.04e-06	4.57 \pm 0.34e-07	7.56 \pm 0.36e-08	4.19 \pm 0.98e-08
NGC3227	2.91 \pm 0.03e-06	9.99 \pm 0.15e-06	1.24 \pm 0.01e-06	3.24 \pm 0.03e-06	1.35 \pm 0.01e-06	5.17 \pm 0.05e-07	2.03 \pm 0.03e-07
NGC3735	5.92 \pm 0.42e-07	3.39 \pm 0.34e-06	5.61 \pm 0.28e-07	7.59 \pm 0.30e-07	4.47 \pm 0.38e-07	5.84 \pm 0.37e-08	2.44 \pm 0.69e-08
NGC4051	8.84 \pm 0.54e-07	4.42 \pm 0.31e-06	3.96 \pm 0.32e-07	1.12 \pm 0.03e-06	5.67 \pm 0.52e-07	1.04 \pm 0.06e-07	8.09 \pm 0.77e-08
NGC4258	3.40 \pm 0.07e-07	1.45 \pm 0.07e-06	1.36 \pm 0.04e-07	3.38 \pm 0.03e-07	1.60 \pm 0.06e-07	7.43 \pm 0.07e-08	6.58 \pm 0.14e-08
NGC4501	1.09 \pm 0.05e-07	3.51 \pm 0.35e-07	8.02 \pm 0.37e-08	3.05 \pm 0.04e-07	1.50 \pm 0.03e-07	4.15 \pm 0.04e-08	6.37 \pm 0.25e-08
NGC4639	9.15 \pm 0.56e-08	2.33 \pm 0.30e-07	3.47 \pm 0.35e-08	1.67 \pm 0.03e-07	6.65 \pm 0.52e-08	9.47 \pm 0.57e-09	9.22 \pm 0.69e-09
NGC4945	7.99 \pm 0.08e-05	3.80 \pm 0.04e-04	3.91 \pm 0.04e-05	2.51 \pm 0.03e-05	2.81 \pm 0.03e-05	5.59 \pm 0.06e-06	3.24 \pm 0.71e-08
NGC5005	1.40 \pm 0.06e-06	5.39 \pm 0.31e-06	1.20 \pm 0.04e-06	3.38 \pm 0.05e-06	1.26 \pm 0.03e-06	3.27 \pm 0.04e-07	4.13 \pm 0.22e-07
NGC5033	6.04 \pm 0.40e-07	2.25 \pm 0.25e-06	4.07 \pm 0.21e-07	1.10 \pm 0.03e-06	5.77 \pm 0.19e-07	1.23 \pm 0.03e-07	4.00 \pm 0.57e-08
NGC5135	5.65 \pm 0.06e-06	2.07 \pm 0.02e-05	3.62 \pm 0.04e-06	4.76 \pm 0.05e-06	2.58 \pm 0.03e-06	8.04 \pm 0.08e-07	1.22 \pm 0.04e-07
NGC5194	2.57 \pm 0.32e-07	6.23 \pm 1.25e-07	1.12 \pm 0.19e-07	6.82 \pm 0.16e-07	2.85 \pm 0.17e-07	1.68 \pm 0.02e-07	1.32 \pm 0.09e-07
NGC5395	6.69 \pm 0.43e-08	2.45 \pm 0.34e-07	4.14 \pm 0.38e-08	1.22 \pm 0.05e-07	5.88 \pm 0.45e-08	4.44 \pm 0.50e-09	6.12 \pm 1.16e-09
NGC5427	2.23 \pm 0.06e-07	1.12 \pm 0.06e-06	1.49 \pm 0.05e-07	2.68 \pm 0.04e-07	1.43 \pm 0.08e-07	4.03 \pm 0.06e-08	1.32 \pm 0.11e-08
NGC5643	1.10 \pm 0.09e-06	4.32 \pm 0.87e-06	4.27 \pm 1.17e-07	1.93 \pm 0.09e-06	9.62 \pm 1.02e-07	1.66 \pm 0.10e-07	7.28 \pm 2.05e-08
NGC5728	9.91 \pm 0.23e-07	5.03 \pm 0.17e-06	7.19 \pm 0.17e-07	2.10 \pm 0.02e-06	8.19 \pm 0.17e-07	2.18 \pm 0.07e-07	1.55 \pm 0.07e-07
NGC6221	9.07 \pm 0.09e-06	3.02 \pm 0.03e-05	4.92 \pm 0.05e-06	6.50 \pm 0.07e-06	3.88 \pm 0.05e-06	1.77 \pm 0.02e-06	1.62 \pm 0.09e-07
NGC6951	1.87 \pm 0.05e-06	6.39 \pm 0.26e-06	1.30 \pm 0.04e-06	2.04 \pm 0.06e-06	9.54 \pm 0.29e-07	2.44 \pm 0.04e-07	8.03 \pm 1.14e-08
NGC7130	2.71 \pm 0.05e-06	1.08 \pm 0.03e-05	1.71 \pm 0.05e-06	2.48 \pm 0.06e-06	1.37 \pm 0.06e-06	5.21 \pm 0.07e-07	6.38 \pm 1.11e-08
NGC7314	1.71 \pm 0.23e-07	1.20 \pm 0.17e-06	1.09 \pm 0.17e-07	2.57 \pm 0.11e-07	1.33 \pm 0.14e-07	6.41 \pm 0.15e-08	2.50 \pm 0.36e-08
NGC7469	8.23 \pm 0.08e-06	2.93 \pm 0.06e-05	4.28 \pm 0.04e-06	5.41 \pm 0.05e-06	3.29 \pm 0.07e-06	1.16 \pm 0.01e-06	1.32 \pm 0.05e-07
NGC7496	2.18 \pm 0.05e-06	6.48 \pm 0.25e-06	1.15 \pm 0.03e-06	1.42 \pm 0.03e-06	7.30 \pm 0.32e-07	2.77 \pm 0.04e-07	6.14 \pm 0.93e-08
NGC7582	2.26 \pm 0.05e-06	8.55 \pm 0.26e-06	2.58 \pm 0.04e-06	4.10 \pm 0.04e-06	1.55 \pm 0.03e-06	3.60 \pm 0.04e-07	1.37 \pm 0.10e-07
NGC7590	3.01 \pm 0.57e-07	1.19 \pm 0.31e-06	2.72 \pm 0.36e-07	4.49 \pm 0.48e-07	1.95 \pm 0.29e-07	2.72 \pm 0.30e-08	2.18 \pm 1.10e-08

NOTE. — Measurements are in units of $\text{W m}^{-2} \text{sr}^{-1}$.

^a Consists of sub-features at 7.42, 7.60, and 7.85 μm .

^b Consists of sub-features at 11.23 and 11.33 μm .

^c Consists of sub-features at 12.62 and 12.69 μm .

TABLE 2
OFF-NUCLEAR MEASUREMENTS

NAME	RA	Dec	6.2 μm	7.7 μm^{a}	8.6 μm	11.3 μm^{b}	12.7 μm^{c}
IC3639	12:40:53.13	-36:45:10.3	4.24 \pm 0.32e-07	1.63 \pm 0.22e-06	1.94 \pm 0.28e-07	2.84 \pm 0.20e-07	1.63 \pm 0.32e-07
NGC1097	02:46:19.06	-30:16:20.0	4.26 \pm 0.07e-06	1.39 \pm 0.04e-05	2.63 \pm 0.05e-06	2.86 \pm 0.05e-06	1.62 \pm 0.03e-06
NGC1365	03:33:36.71	-36:08:18.0	8.53 \pm 0.09e-06	3.37 \pm 0.04e-05	6.68 \pm 0.08e-06	6.24 \pm 0.07e-06	4.15 \pm 0.05e-06
NGC1566	04:20:02.13	-54:56:37.1	2.69 \pm 0.18e-07	8.33 \pm 1.14e-07	1.16 \pm 0.13e-07	1.33 \pm 0.10e-07	7.92 \pm 1.39e-08
NGC2992	09:45:42.07	-14:19:29.4	1.05 \pm 0.10e-06	3.59 \pm 0.75e-06	6.48 \pm 0.84e-07	9.31 \pm 1.03e-07	6.07 \pm 0.47e-07
NGC3079	10:01:57.49	+55:40:58.5	2.61 \pm 0.10e-06	9.02 \pm 0.30e-06	1.58 \pm 0.09e-06	1.80 \pm 0.08e-06	9.90 \pm 0.27e-07
NGC3227	10:23:30.87	+19:51:43.1	1.04 \pm 0.08e-07	4.36 \pm 0.43e-07	7.23 \pm 0.46e-08	1.51 \pm 0.07e-07	7.30 \pm 0.49e-08
NGC4258	12:18:59.31	+47:18:24.8	4.44 \pm 0.05e-07	1.44 \pm 0.02e-06	2.60 \pm 0.03e-07	2.87 \pm 0.03e-07	1.51 \pm 0.04e-07
NGC4501	12:32:00.42	+14:25:25.2	2.97 \pm 0.08e-07	1.09 \pm 0.03e-06	1.92 \pm 0.05e-07	2.43 \pm 0.06e-07	1.33 \pm 0.04e-07
NGC4945	13:05:28.26	-49:27:39.6	2.24 \pm 0.06e-06	7.69 \pm 0.11e-06	1.61 \pm 0.07e-06	1.72 \pm 0.06e-06	9.13 \pm 0.19e-07
NGC5005	13:10:56.89	+37:03:24.8	4.87 \pm 0.65e-07	1.98 \pm 0.50e-06	3.28 \pm 0.32e-07	4.59 \pm 0.25e-07	2.71 \pm 0.34e-07
NGC5033	13:13:27.87	+36:35:25.6	9.14 \pm 0.28e-07	3.47 \pm 0.15e-06	6.73 \pm 0.34e-07	7.55 \pm 0.23e-07	4.72 \pm 0.21e-07
NGC5135	13:25:44.60	-29:50:08.6	1.90 \pm 0.13e-07	8.02 \pm 0.97e-07	1.31 \pm 0.09e-07	2.24 \pm 0.07e-07	1.27 \pm 0.25e-07
NGC5194	13:29:50.36	+47:11:36.0	7.64 \pm 0.25e-07	2.82 \pm 0.11e-06	4.08 \pm 0.24e-07	5.82 \pm 0.19e-07	3.60 \pm 0.20e-07
NGC5395	13:58:38.82	+37:25:38.2	2.49 \pm 0.04e-07	8.21 \pm 0.31e-07	1.47 \pm 0.04e-07	1.61 \pm 0.03e-07	8.41 \pm 0.56e-08
NGC5427	14:03:26.11	-06:01:43.2	2.64 \pm 0.07e-07	1.02 \pm 0.05e-06	1.87 \pm 0.05e-07	2.24 \pm 0.04e-07	1.24 \pm 0.07e-07
NGC6221	16:52:46.03	-59:13:08.8	1.05 \pm 0.04e-06	3.04 \pm 0.19e-06	6.22 \pm 0.25e-07	1.21 \pm 0.04e-06	6.46 \pm 0.31e-07
NGC7130	21:48:19.38	-34:56:56.1	1.31 \pm 0.03e-06	4.35 \pm 0.13e-06	8.07 \pm 0.25e-07	1.03 \pm 0.03e-06	5.14 \pm 0.14e-07
NGC7314	22:35:46.89	-26:03:13.7	1.11 \pm 0.13e-07	4.55 \pm 1.01e-07	8.01 \pm 1.30e-08	1.00 \pm 0.10e-07	5.26 \pm 1.40e-08
NGC7582	23:18:22.64	-42:21:57.7	4.14 \pm 0.29e-07	1.82 \pm 0.19e-06	2.29 \pm 0.24e-07	3.36 \pm 0.18e-07	1.76 \pm 0.31e-07
NGC7590	23:18:55.05	-42:14:28.0	5.19 \pm 0.53e-07	1.78 \pm 0.37e-06	2.81 \pm 0.29e-07	3.58 \pm 0.22e-07	1.79 \pm 0.29e-07

NOTE. — Measurements are in units of $\text{W m}^{-2} \text{sr}^{-1}$.^a Consists of sub-features at 7.42, 7.60, and 7.85 μm .^b Consists of sub-features at 11.23 and 11.33 μm .^c Consists of sub-features at 12.62 and 12.69 μm .TABLE 3
STATISTICAL TESTS

ratio	Seyferts v. SINGS	Seyferts v. off nuclear	SINGS v. off nuclear
6/11	5×10^{-4}	5×10^{-5}	0.682
7/11	0.003	0.001	0.074
8/11	9×10^{-4}	2×10^{-4}	0.063
6/7	0.230	0.447	0.888
6/8	0.489	0.347	0.689
7/8	0.108	0.303	0.374

NOTE. — Values correspond to probabilities from two-sample K-S tests.